

FAR ULTRAVIOLET SPECTROSCOPIC EXPLORER SPECTROSCOPY OF ABSORPTION AND EMISSION LINES FROM THE NARROW-LINE SEYFERT 1 GALAXY NGC 4051

SHAI KASPI,^{1,2} W. N. BRANDT,³ M. J. COLLINGE,⁴ MARTIN ELVIS,⁵ AND CHRISTOPHER S. REYNOLDS⁶

Received 2003 December 12; accepted 2004 February 11

ABSTRACT

We present three *Far Ultraviolet Spectroscopic Explorer (FUSE)* observations of the Narrow-Line Seyfert 1 galaxy NGC 4051. The most prominent features in the far-ultraviolet (FUV) spectrum are the O VI emission and absorption lines and the H I Lyman series absorption lines which are detected up to the Lyman edge. We also identify weak emission from N III, C III, and He II. The C III line shows absorption while none is detected in the N III and He II lines. In H I and C III we detect two main absorption systems at outflow velocities of -50 ± 30 and -240 ± 40 km s⁻¹, as well as a possible third one at ~ -450 km s⁻¹. These systems are consistent in velocity with the 10 absorption systems found previously in C IV, N V, and Si IV, though the individual systems are blended together in the FUV spectrum. We estimate column densities of the two main absorption systems and find that the H I column density is lower for systems with larger outflow velocity. We detect no flux or spectral variations of NGC 4051 at FUV wavelengths during three epochs spanning one year. This is consistent with the optical light curve which shows no variations between the three epochs. It is also consistent with the X-ray light curve which shows consistent flux levels at the three epochs of the *FUSE* observations, although the X-ray light curve shows strong variations on much shorter timescales.

Subject headings: galaxies: active — galaxies: individual (NGC 4051) — galaxies: nuclei — galaxies: Seyfert — techniques: spectroscopic — ultraviolet: galaxies

1. INTRODUCTION

The Narrow-Line Seyfert 1 (NLS1) galaxy NGC 4051 is one of the best-studied active galactic nuclei (AGN) across the electromagnetic spectrum due to its brightness and proximity ($V \approx 13.5$; $z = 0.002295 \pm 0.000043$ from optical emission lines; de Vaucouleurs et al. 1991). It has been part of many studies since it was first mentioned by Hubble (1926) and classified by Seyfert (1943). Collinge et al. (2001) recently presented the first high-resolution X-ray and ultraviolet (UV) spectra of NGC 4051. The *Chandra* High-Energy Transmission Grating Spectrometer (HETGS) spectrum reveals absorption and emission lines from hydrogen-like and helium-like ions of O, Ne, Mg, and Si. Two distinct blueshifted absorption systems were detected: a high-velocity system at -2340 ± 130 km s⁻¹ and a low-velocity system at -600 ± 130 km s⁻¹. In a *Chandra* Low-Energy Transmission Grating Spectrometer (LETGS) observation taken ~ 2 yr later, van der Meer et al. (2003) claim to detect a new X-ray absorption system at ~ -4500 km s⁻¹ while the -2340 km s⁻¹ system is barely visible. An even higher velocity outflowing absorption system at ~ -6500 km s⁻¹ or ~ -16500 km s⁻¹ (depending on the identification of an absorption line at 7.1 keV in an *XMM-Newton* EPIC observation) was suggested recently by Pounds et al. (2003). The UV spectrum taken with the Space Telescope Imaging Spectrograph (STIS) shows strong absorption mainly in the lines of C IV, N V, and Si IV. Ten

intrinsic UV absorption systems are seen with velocities between -650 and 30 km s⁻¹ and FWHMs ranging from ~ 30 to ~ 160 km s⁻¹. While the low-velocity X-ray absorption system is consistent in velocity with many of the UV absorption systems, the high-velocity X-ray absorption seems to have no UV counterpart.

NGC 4051 shows rapid and large-amplitude X-ray flux variability by up to an order of magnitude on timescales of hours (e.g., Marshall et al. 1983; Uttley et al. 2000; Collinge et al. 2001; McHardy et al. 2003; and references therein). Uttley et al. (2000) found a strong correlation between the variability in the extreme UV (124–188 eV) and X-ray (2–10 keV) bands, and they suggested this to indicate that both bands are sampling the same power-law continuum. Shemmer et al. (2003) find the variable optical continuum flux to correlate with the variable X-ray flux. The optical continuum leads the X-ray by 2.4 ± 1.0 days. They also found that the variation amplitude in the optical is much smaller than in the X-ray, as seen in other NLS1s.

In this paper we bridge between the X-ray and near UV high-resolution spectra by presenting the first *Far Ultraviolet Spectroscopic Explorer (FUSE)* spectra of NGC 4051. The *FUSE* spectra cover the 900–1180 Å band with a resolution of ~ 0.06 Å (corresponding to ~ 20 km s⁻¹). Our main proposed goals were (1) to study the FUV kinematic counterparts to the known X-ray and UV absorption lines, (2) to study any FUV absorption-line variability, and (3) to relate any FUV variability to that seen at X-ray and other wavelengths. The observations and data reduction are detailed in § 2. In §§ 3 and 4 we present the temporal and spectral analyses, and in § 5 we discuss our results. Finally, § 6 presents a summary of our main results.

2. OBSERVATIONS AND DATA REDUCTION

NGC 4051 was observed with *FUSE* (Moos et al. 2000; Sahnou et al. 2000) during three epochs, spanning one year, which are listed in Table 1. The observations were carried

arXiv:astro-ph/0402318v1 13 Feb 2004

¹ School of Physics and Astronomy, Raymond and Beverly Sackler Faculty of Exact Sciences, Tel-Aviv University, Tel-Aviv 69978, Israel; shai@wise.tau.ac.il

² Physics Department, Technion, Haifa 32000, Israel.

³ Department of Astronomy & Astrophysics, 525 Davey Laboratory, The Pennsylvania State University, University Park, PA 16802, USA.

⁴ Princeton University Observatory, Princeton, NJ 08544, USA.

⁵ Harvard-Smithsonian Center for Astrophysics, 60 Garden Street, Cambridge, MA 02138, USA.

⁶ Department of Astronomy, University of Maryland, College Park, MD 20742, USA.

TABLE 1
FUSE OBSERVATION LOG FOR NGC 4051

Obs. ID	Date and UT	N_{orbits}^a	Time (ks) ^b
B0620201000	2002 Mar 29 01:58	21	28.7
C0190101000	2003 Jan 18 11:43	16	34.7
C0190102000	2003 Mar 19 07:46	17	28.8

^aNumber of consecutive orbits.

^bTotal effective exposure time.

out using the $30'' \times 30''$ low-resolution (LWRS) aperture in the standard observing mode. Each observation consists of several consecutive orbits, and in each orbit data from eight detectors (each covering a different wavelength range) were accumulated. We reduced the raw data using the most recent *FUSE* software (CalFUSE v2.4.0 and the *FUSE* IDL tools version of 2002 July). For each observation we checked the data from different detectors and orbits for consistency and found no significant deviations in flux. Hence, we used the FUSE_REGISTER tool to combine the data sets from the different detectors and orbits into one spectrum per observation.

In the following analysis we use the line templates from Feldman et al. (2001) to identify the airglow geocoronal emission lines and Sembach (1999) to identify interstellar Galactic absorption lines.

3. TEMPORAL ANALYSIS

Visual comparison of the spectra from the three epochs suggests striking similarity between them with no apparent time variation of the intrinsic spectrum. To assess any time variations quantitatively, we computed $(f_1 - f_2) / \sqrt{(\sigma_1^2 + \sigma_2^2)}$ for each pair of spectra, where f_1 and f_2 are the flux densities at a given wavelength and σ_1 and σ_2 are their uncertainties. Plots of this quantity versus wavelength revealed that the only variable regions in the spectra (including regions where absorption lines are present) could be explained by variable geocoronal emission lines or uncertainties in calibration. We also measured the average flux densities of the three spectra in several wavelength bands which are free from emission and absorption; these measurements are listed in Table 2 and confirm that there are no variations within the $\sim 10\%$ uncertainty of each measurement. A careful look at Table 2 suggests that the flux of the 2002 Mar 29 spectrum may be somewhat lower (by $\sim 3\%$) than for the two spectra taken about a year later, especially longward of $\sim 990 \text{ \AA}$. However, this possible variation is not highly significant ($\lesssim 1\sigma$). Since we found the spectra from the three epochs to be consistent, we combined them into one 92.2 ks spectrum to increase the S/N of our analysis (see Figure 1).

We also checked for flux variations within each observation by comparing the spectra between single orbits and by combining 4–5 orbits together. The spectra from single orbits have very poor S/N (of order 1), and no variability is detected between them within the limiting S/N of the data. Analyses of the spectra made by combining 4–5 orbits together show that any FUV variability is less than $\sim 20\%$ (considering several wavelength bands as given in Table 2).

We compared the *FUSE* observations to the long-term *RXTE* 2–10 keV light curve of NGC 4051 (Lamer et al. 2003; McHardy et al. 2003; P. Uttley and I. M. McHardy 2003, private communication). During the year of the *FUSE* obser-

TABLE 2
AVERAGE FLUX-DENSITY MEASUREMENTS

Wavelength range ^a	2002 Mar 29 ^b	2003 Jan 18 ^b	2003 Mar 19 ^b
926.5–927.2	13.39 ± 1.22	13.86 ± 1.21	13.37 ± 1.23
939.8–941.8	11.01 ± 0.76	10.95 ± 0.70	10.29 ± 0.73
956.9–958.0	13.09 ± 1.09	12.61 ± 0.98	13.18 ± 1.07
967.1–968.2	9.28 ± 1.10	10.69 ± 1.02	8.92 ± 1.05
998.2–999.2	13.93 ± 1.04	16.81 ± 0.94	15.24 ± 1.01
1019.2–1020.7	15.45 ± 0.72	16.92 ± 0.64	16.56 ± 0.69
1030.1–1031.6 ^c	7.81 ± 0.62	8.31 ± 0.56	8.15 ± 0.59
1042.0–1043.0 ^d	21.38 ± 0.90	21.69 ± 0.79	21.33 ± 0.87
1056.1–1057.6	12.76 ± 0.76	14.36 ± 0.67	13.16 ± 0.71
1069.0–1070.0	13.29 ± 0.97	14.42 ± 0.85	14.50 ± 0.92
1089.0–1090.0	12.22 ± 1.65	13.33 ± 1.33	11.29 ± 1.34
1095.0–1096.5	9.98 ± 0.87	11.88 ± 0.72	11.69 ± 0.75
1114.4–1116.4	10.79 ± 0.37	11.97 ± 0.33	10.99 ± 0.35
1127.4–1129.4	9.59 ± 0.36	11.41 ± 0.33	10.75 ± 0.35
1145.4–1147.4	8.97 ± 0.41	9.17 ± 0.34	9.50 ± 0.38
1181.3–1183.3	13.30 ± 0.96	14.04 ± 0.80	13.56 ± 0.88

^aIn units of \AA in the rest frame.

^bIn units of $10^{-15} \text{ erg cm}^{-2} \text{ s}^{-1} \text{ \AA}^{-1}$.

^cMeasurement in the trough of O VI $\lambda 1032$.

^dMeasurement on the red wing of O VI $\lambda 1038$.

vations, NGC 4051 was observed with *RXTE* every two days allowing fairly contemporaneous comparison of the X-ray and FUV fluxes (although, as noted in § 1, NGC 4051 is highly X-ray variable on even shorter timescales). The fluxes from the three *RXTE* observations closest in time to the *FUSE* observations are consistent [the 2–10 keV fluxes are measured to lie in the range $(3\text{--}3.5) \times 10^{-11} \text{ erg cm}^{-2} \text{ s}^{-1}$]. We also compared the *FUSE* observations to optical observations taken on similar dates (within about 10 days) at the Wise Observatory. The optical observations show no variations either. This is consistent with the results of Peterson et al. (2000) and Shemmer et al. (2003) who find NGC 4051 to vary by only a few percent in the optical.

4. SPECTRAL ANALYSIS

The most prominent intrinsic features seen in the *FUSE* spectrum (Figure 1) are the O VI emission and absorption lines and the H I Lyman series absorption lines, which are detected up to the Lyman edge. We also identify weak intrinsic emission from N III, C III, and He II. The C III line shows absorption, while no intrinsic absorption is detected in the N III and He II lines. All absorption lines are blueshifted relative to the systemic velocity, and some show multiple absorption systems.

To study the intrinsic O VI absorption, we fitted each of the two doublet emission lines with two Gaussians, keeping the width of each Gaussian the same for both doublet lines and keeping the flux ratio the same as the oscillator-strength ratio (2:1). The fit results are shown in Figure 2 and listed in Table 3. The observed spectrum was then divided by this emission model, and the resulting normalized spectrum was used to create the absorption velocity spectra shown in Figure 3a. The absorption-line profiles of the two O VI lines are similar with no noticeable features in the trough which ranges from about 50 km s^{-1} to -800 km s^{-1} . The overall spread of velocities is in agreement with the 10 absorption systems identified in the UV lines of C IV and N V (see Figure 3b); however, no individual absorption systems are seen in O VI. Since the resolution of the FUV spectrum is high enough to resolve these systems at least in part (see Figure 3c), and since

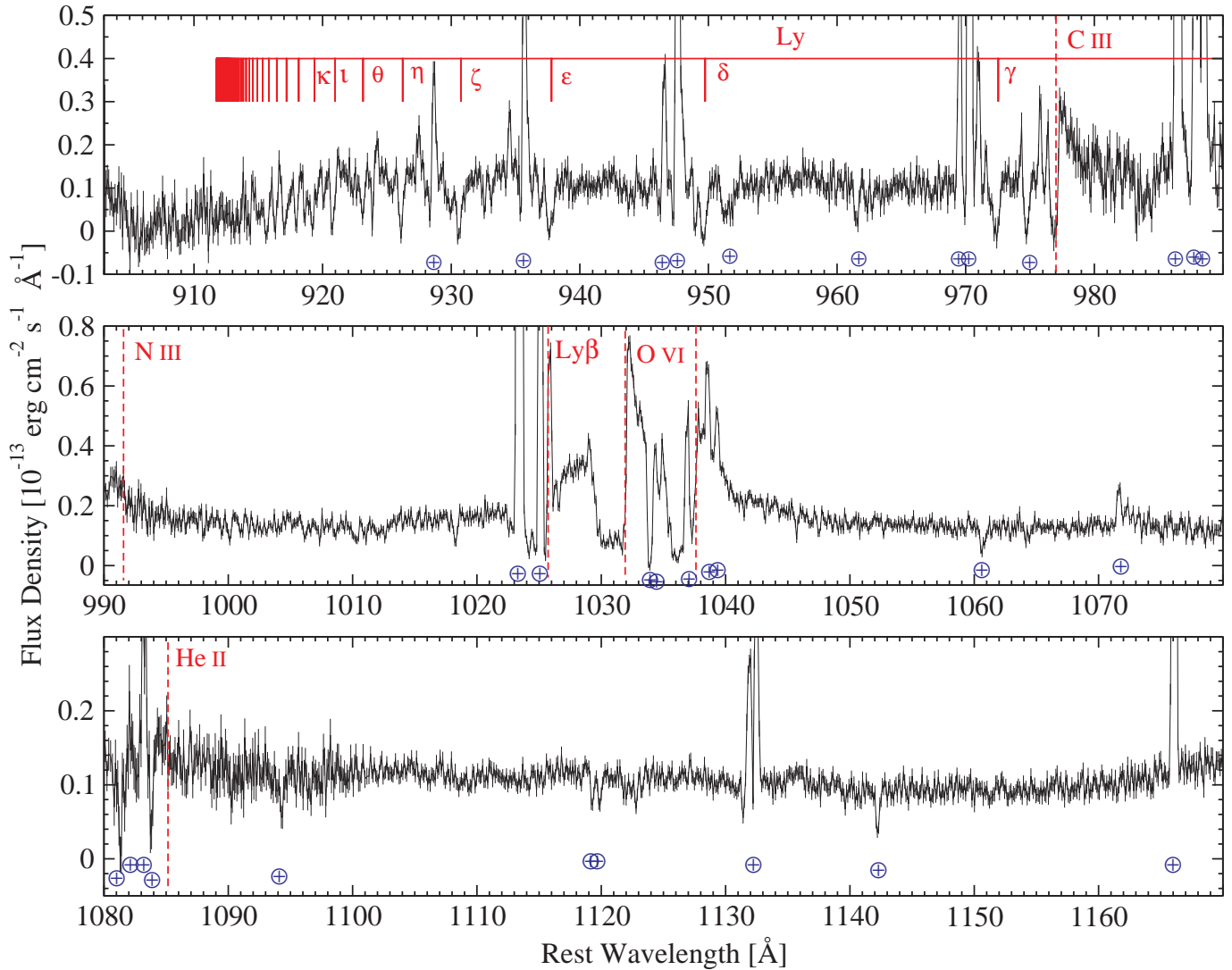


FIG. 1.— The combined 92.2 ks *FUSE* spectrum of NGC 4051 binned to $\sim 0.1 \text{ \AA pix}^{-1}$. Intrinsic emission lines are marked at their theoretically expected positions in red above the spectrum. Airglow geocoronal emission lines and interstellar Galactic absorption lines are marked with \oplus . The intrinsic H I absorption lines are marked at their theoretically expected positions up to the ionization energy in the top panel.

the troughs of the two lines have similar depths (thus departing from the oscillator-strength ratio), we conclude that the O VI absorption lines are saturated and have broad enough damping wings to create a single trough. The O VI trough is not completely black which indicates partial covering of this absorber.⁷ From Figure 3a we estimate the absorber covering factor to be $\sim 0.9\text{--}0.95$.

In addition to its FUV lines, the ion O VI is also expected to have X-ray absorption lines at 19.135, 19.341, 21.79, and 22.01 Å (E. Behar 2003, private communication; see also Pradhan 2000). The O VI $\lambda\lambda 1032, 1038$ absorption systems detected in the *FUSE* spectrum have a combined width of $\sim 700 \text{ km s}^{-1}$. The velocity resolution of the *Chandra* HETGS (LETGS) spectrum, at $\sim 20 \text{ \AA}$, is ~ 350 (600) km s^{-1} ; hence the O VI absorption lines can be resolved by these instruments. Examination of the HETGS and LETGS spec-

⁷ We rule out the possibility that the trough is not black due to an instrumental scattering problem since the Galactic absorption line at $\sim 1034 \text{ \AA}$ reaches zero flux. We also rule out the possibility of scattering of nuclear light into the line of sight since other absorption lines reach zero flux; see the discussion at the end of § 5.1.

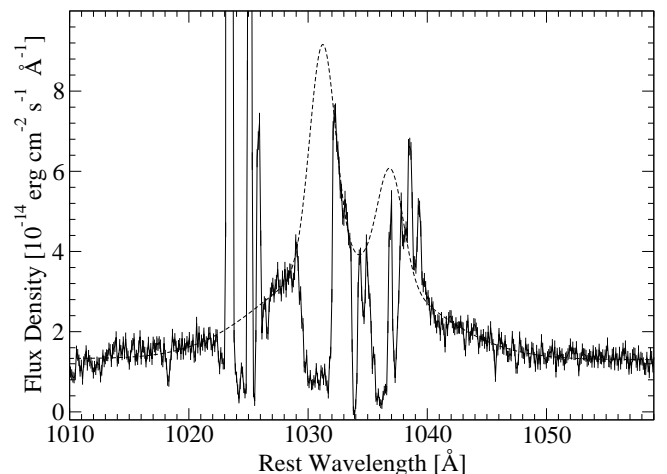


FIG. 2.— Fit to the O VI emission lines using two Gaussians for each line (dashed curve) plotted over the *FUSE* spectrum (solid curve) which is binned to $\sim 0.1 \text{ \AA pix}^{-1}$. The 1σ uncertainties for the points are also shown. The fit parameters are given in Table 3.

TABLE 3
O VI FIT PARAMETERS

Gaussian	Normalization ^a	σ^b [\AA]	FWHM ^b [km s^{-1}]
I	0.540	1.074	735
II	0.179	5.831	3970

NOTE. — All Gaussian centroids were set to the same velocity. In the rest-frame spectrum of the source they correspond to 1031.22 \AA and 1036.91 \AA , i.e., the fitted O VI emission lines are blueshifted by -200 km s^{-1} relative to the optical lines.

^aThe O VI $\lambda 1032$ line normalization in units of $10^{-13} \text{ erg cm}^{-2} \text{ s}^{-1} \text{ \AA}^{-1}$. The O VI $\lambda 1038$ line normalization was set to half the O VI $\lambda 1032$ line normalization.

^b σ and FWHM are the same for the two lines of the doublet.

tra shows that the data are consistent with these lines being present, though the poor S/N prevents any significant detection.

In Figure 3c we compare the absorption profile of C III with that of C IV $\lambda 1550$ from Collinge et al. (2001). C III shows absorption in the velocity ranges of -150 to 50 , -330 to -230 , and possibly around -450 km s^{-1} . Within the limitations of the FUV spectral resolution ($\sim 20 \text{ km s}^{-1}$), the main absorption systems that were identified in the C IV STIS profile are also seen in the C III *FUSE* profile. The recession velocity of NGC 4051 is $\sim +690 \text{ km s}^{-1}$. Any absorption at an apparent rest-frame blueshifted velocity of $\sim -690 \text{ km s}^{-1}$ is probably Galactic or contaminated by Galactic absorption, and no useful information about the intrinsic absorption in NGC 4051 can be deduced from absorption near this velocity.

Velocity spectra for the first eight lines in the H I Lyman series are shown in Figure 4. The Ly α absorption observed with STIS (from Collinge et al. 2001) is shown in Figure 4a together with Ly β from *FUSE*. Ly α does not show individual intrinsic systems but rather has a broad absorption trough which reaches up to a velocity of $\sim -1200 \text{ km s}^{-1}$. All the Lyman series lines observed with *FUSE* show geocoronal Lyman emission lines at ~ -550 to -750 km s^{-1} . The absorption trough of Ly β is further contaminated with geocoronal O I lines which mask the absorption in the range ~ 90 to -270 km s^{-1} . The Ly γ and Ly δ lines are shown in Figure 4b. Both lines are contaminated at velocities $\lesssim -430 \text{ km s}^{-1}$.

The H I Lyman absorption lines are seen all the way to the Lyman edge (see Figure 1 top panel and Figure 5). We identify two main H I Lyman absorption systems: one at $-50 \pm 30 \text{ km s}^{-1}$ which is detected in the lines from Ly γ to Ly ξ (after which the lines are blended together and blended with airglow emission lines; see Figure 5), and one at $-240 \pm 40 \text{ km s}^{-1}$ which is detected in the lines from Ly γ to Ly λ (after which it is weak and blended with the -50 km s^{-1} absorption lines). All lines identified in the -50 km s^{-1} system are saturated.

We used the XVOIGT software (Mar & Bailey 1995) to estimate the column densities of the two H I Lyman absorption systems. XVOIGT allows the interactive fitting of Voigt profiles to atomic absorption lines in astronomical spectra. We fitted simultaneously all identified lines in each system in order to determine the column densities and the Doppler widths of the systems, assuming that each system is formed by a single absorber. The large number of lines fitted in each system allowed us to fit even the saturated lines, using the differences in their saturated Voigt profiles. We find the -50

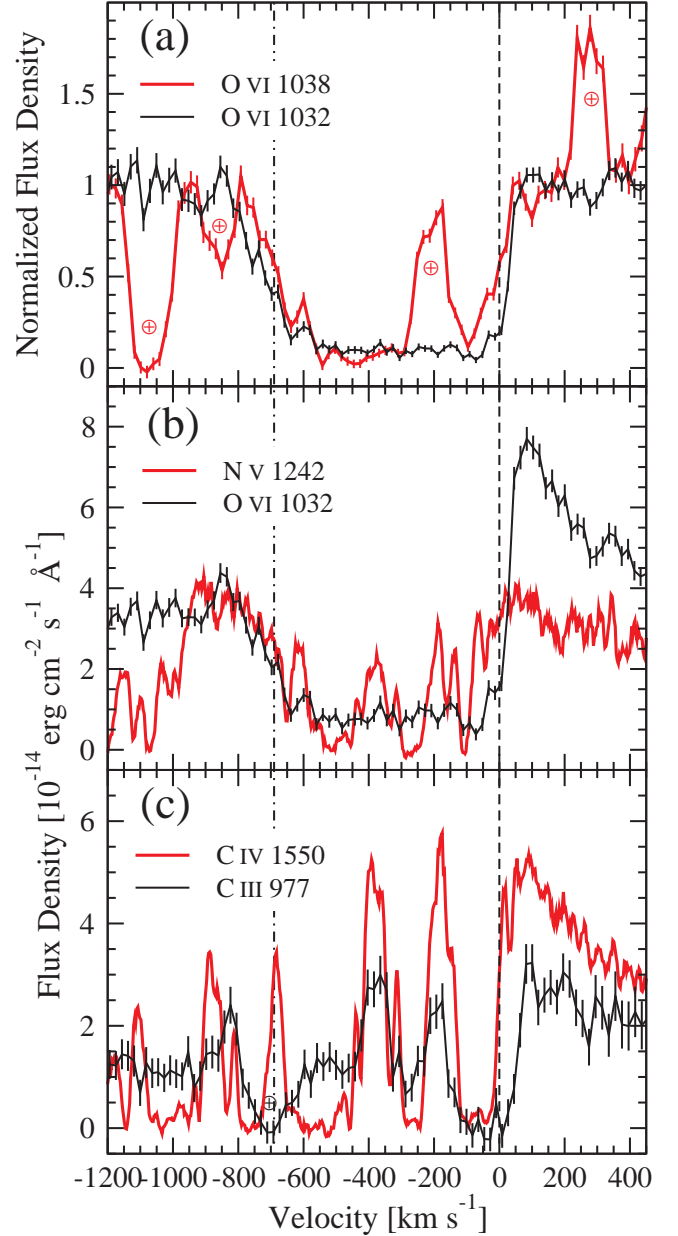


FIG. 3.— (a) Velocity spectra for the two normalized O VI lines. Airglow geocoronal emission lines and interstellar Galactic absorption lines are marked with \oplus . The dashed line marks the rest frame zero velocity and the dotted-dashed line marks the recession velocity of NGC 4051, i.e., absorption around this velocity is suspected to be Galactic. (b) Velocity spectrum comparison between the O VI $\lambda 1032$ line and the N V $\lambda 1242$ line from Collinge et al. (2001). The individual N V $\lambda 1242$ absorption systems are blended into one wide trough in the O VI $\lambda 1032$ line. (c) Velocity spectrum comparison between the C III $\lambda 977$ line and the C IV $\lambda 1550$ line from Collinge et al. (2001). The flux of the C IV $\lambda 1550$ spectrum was scaled by 0.5 for clarity of the plot. There is a good correlation between the absorption systems seen in both ions, though the C III $\lambda 977$ spectrum has poorer resolution. Not all 10 absorption systems seen in C IV $\lambda 1550$ can be identified in the C III $\lambda 977$ absorption, though the C III profile is consistent with all 10 systems being present.

km s^{-1} system to have a column density of $2.2^{+1.3}_{-1.1} \times 10^{17} \text{ cm}^{-2}$ and the -240 km s^{-1} system to have a column density of $1.0^{+0.6}_{-0.5} \times 10^{16} \text{ cm}^{-2}$; we note that these column density estimates could have significant systematic errors if there is unresolved velocity substructure in the lines. For both systems we find a Doppler width of $b = 35 \pm 15 \text{ km s}^{-1}$. Shortward of the Lyman edge the flux drops to about 30% of the

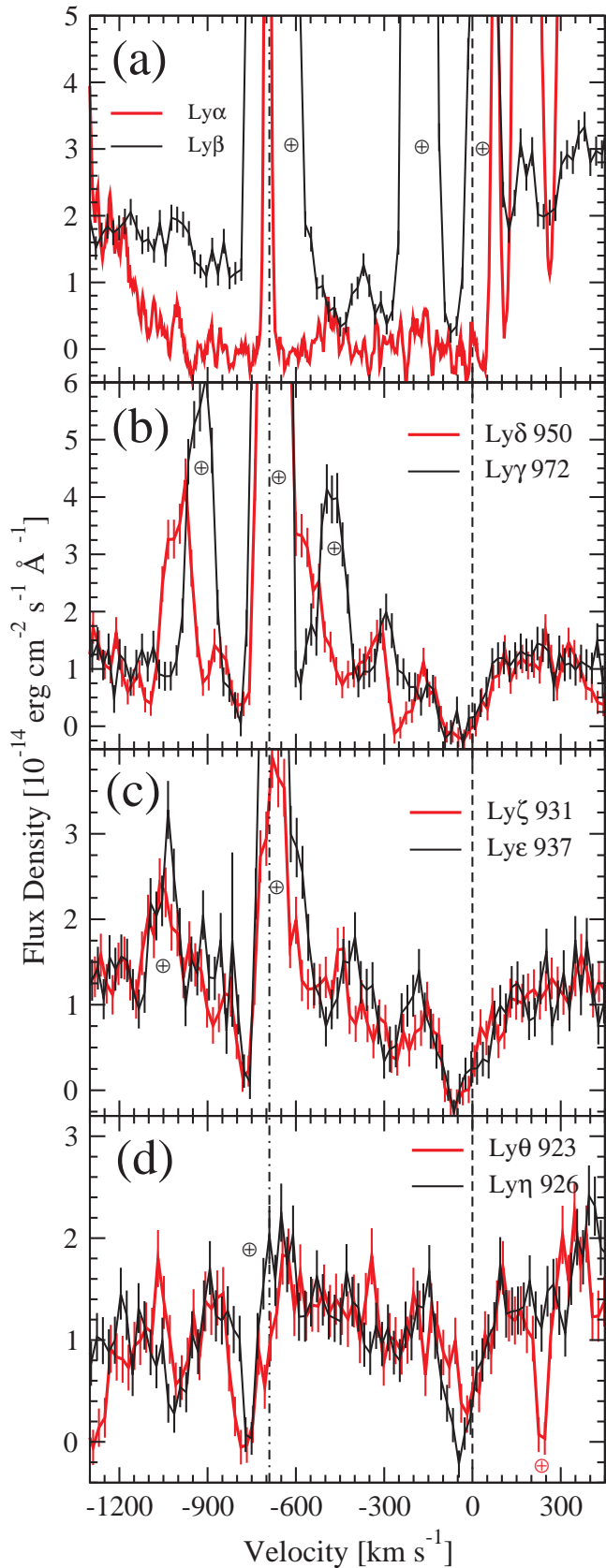


FIG. 4.— Velocity spectra for the first eight lines in the H I Lyman series. The vertical dashed line marks zero velocity. Airglow geocoronal emission lines and interstellar Galactic absorption lines are marked with \oplus . The dashed line marks the rest frame zero velocity and the dotted-dashed line marks the recession velocity of NGC 4051, i.e., absorption around this velocity is suspected to be Galactic.

continuum value. This can be explained by the total column density found above ($\sim 2.3 \times 10^{17} \text{ cm}^{-2}$) which can produce such Lyman continuum absorption. The Galactic Lyman edge appears at 909.7 \AA in the NGC 4051 rest-frame spectrum (see Figure 5), and shortward of it the spectrum is totally absorbed.

There is probably yet another absorption system of H I at around -400 to -500 km s^{-1} . This system is seen only in Ly β , Ly δ , Ly ϵ , and possibly Ly ζ (Figure 4). This absorption is shallower than the other two systems and is seen only in 3–4 lines; hence we cannot measure its low column density as for the other two systems.

Two Ly α absorption systems with redshift velocities of ~ 110 and $\sim 260 \text{ km s}^{-1}$ were suggested by Collinge et al. (2001) to originate in low-ionization, high-velocity clouds within NGC 4051 (see their Figure 9). These are also identified in Ly β absorption and marginally identified in Ly γ and Ly δ (Figure 4a and 4b).

In the HETGS spectrum of NGC 4051, Collinge et al. (2001) found a high-velocity absorption system at -2340 km s^{-1} . We also looked for this system in the *FUSE* spectrum. For the O VI $\lambda 1032$ line this high-velocity absorption system falls in the Ly β absorption trough where it is blended with geocoronal emission. For the O VI $\lambda 1038$ line this absorption system falls on the blue wing of the O VI $\lambda 1032$ trough. Figure 3a shows that the blue wings of the two O VI troughs are similar, although the blue wing for O VI $\lambda 1032$ is a bit lower than for O VI $\lambda 1038$. However, this difference is not significant enough to claim a detection since such a small discrepancy could be caused by calibration effects or by uncertainties in the fit to the O VI emission. We also do not detect the -4500 km s^{-1} absorption system reported by van der Meer et al. (2003) from the *Chandra* LETGS spectrum, nor do we detect the $\sim -6500 \text{ km s}^{-1}$ or $\sim -16500 \text{ km s}^{-1}$ (depending on the interpretation of an absorption line seen at $\sim 7.1 \text{ keV}$) absorption system reported by Pounds et al. (2003) from an *XMM-Newton* observation.

5. DISCUSSION

5.1. Far Ultraviolet Emission and Absorption

In these first FUV spectra of NGC 4051, we detect emission from O VI, N III, He II, and C III. The O VI emission lines are fitted with two Gaussians with FWHMs of ~ 700 and $\sim 4000 \text{ km s}^{-1}$; the overall line profiles are significantly broader than for the optical lines. This is in agreement with the majority of other NLS1s which show broad wings (several thousands of km s^{-1}) on their high-ionization UV lines (e.g., Rodríguez-Pascual, Mas-Hesse, & Santos-Lleo 1997). We also find the Gaussian centroids to be blueshifted by -200 km s^{-1} relative to the optical lines. This is again in agreement with the findings for other AGN (e.g., Richards et al. 2002 and references therein).

We detect absorption on the blue wings of the O VI and C III emission lines, as well as absorption in the H I Lyman series. In H I we identify two main absorption systems and possibly a third at outflow velocities of -50 ± 30 , -240 ± 40 , and $\sim -450 \text{ km s}^{-1}$. These three absorption systems are also present in C III (Figure 3c). The three FUV systems correspond in outflow velocity to UV systems 7–8, 5, and 2–3 which were found by Collinge et al. (2001) in N V, Si IV, and C IV. Thus, it is plausible that each of the three systems detected in the FUV is a blend of several narrower systems which cannot be resolved by *FUSE*.⁸

⁸ We note that UV system 5 (and perhaps other systems) of Collinge et al.

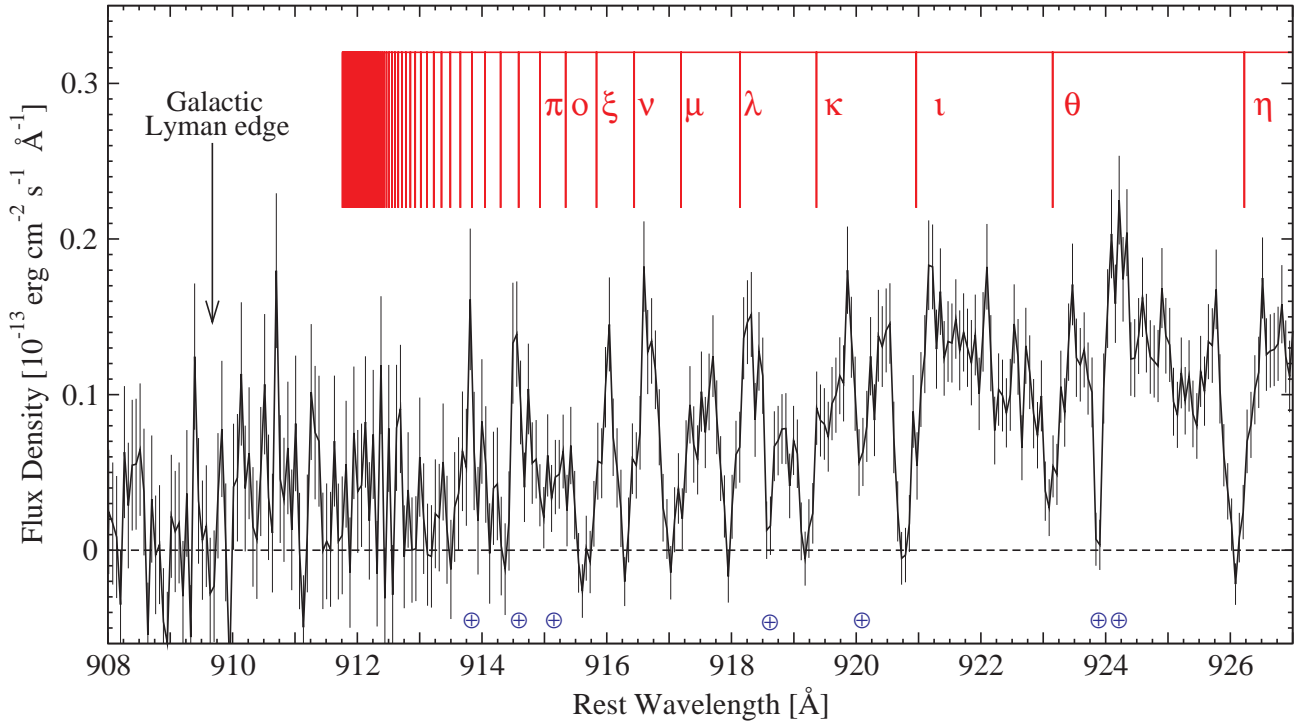


FIG. 5.— The combined 92.2 ks *FUSE* spectrum of NGC 4051 binned to $\sim 0.07 \text{ \AA pix}^{-1}$ showing the Lyman absorption lines of H I toward the Lyman limit. All absorption lines up to Ly ξ appear to be saturated and are blueshifted by -50 km s^{-1} . The Galactic Lyman limit absorption starts at 909.7 \AA . The dashed horizontal line shows the zero flux level. Airglow geocoronal emission lines and interstellar Galactic absorption lines are marked with \oplus .

An interesting relation is present between the strengths of the absorption systems and their outflow velocities. The absorption system with the largest outflow velocity ($\sim -450 \text{ km s}^{-1}$) seems to have the weakest absorption, and it is present only in the lines up to about Ly ζ , i.e., it has a relatively low column density. The absorption system with the smallest outflow velocity ($\sim -50 \text{ km s}^{-1}$) has the strongest absorption with relatively high column density ($2.2^{+1.3}_{-1.1} \times 10^{17} \text{ cm}^{-2}$), and all the lines that can be detected within the limit of the instrumental resolution (up to Ly ξ) are saturated. The intermediate-velocity absorption system (at $\sim -250 \text{ km s}^{-1}$) has an intermediate absorption depth, detected only up to Ly λ , and it has a column density of $1.0^{+0.6}_{-0.5} \times 10^{16} \text{ cm}^{-2}$. This relation might be explained if the systems with higher velocities are closer to the central radiation source and hence are in a more intense radiation field which yields less H I in these systems. This might indicate that the outflow is decelerating so that its velocity decreases as its distance from the ionizing source increases (a decelerating outflow was also found recently in NGC 3783; Gabel et al. 2003). In the lowest velocity outflow system, which is highly saturated, we detect on the trough’s wing from 100 to -100 km s^{-1} the effect of a velocity dependent covering factor (see Figure 3a), i.e., the absorption profile is produced by a different covering factor for each outflow velocity and not by the internal Voigt profiles of the lines (e.g., Arav, Korista, & de Kool 2002).

We can use the multi-epoch observations to put some constraints on the line-of-sight acceleration of the absorbers.⁹

(2001) is saturated and broad; hence it might well be a blend of several systems which are intrinsically blended (rather than just blended due to instrumental resolution).

⁹ This might not be the physical acceleration of the absorbing material, which could be crossing our line of sight to the nucleus in a “standing” pattern.

First we use the *FUSE* observations which are separated by 354.4 days in the rest frame. An upper limit on the absorption profile difference between the two epochs is 30 km s^{-1} (this is the trough location measurement uncertainty; here we used the O VI, C III, and Ly γ to Ly θ absorption lines). Thus, the upper limit on the acceleration of the absorber is $9.8 \times 10^{-7} \text{ km s}^{-2}$. Next we used the time between the STIS observation and the last *FUSE* observation which is 1086.9 days in the rest frame. From the observed consistency of 100 km s^{-1} between the two (e.g., Figure 3b), we derive an upper limit on the absorber’s acceleration of $1.1 \times 10^{-6} \text{ km s}^{-2}$. The upper limit we find is at the lower range of the UV-outflow deceleration discovered recently in NGC 3783 of $\sim (1-2.5) \times 10^{-6} \text{ km s}^{-2}$ (Gabel et al. 2003).

The O VI absorption we detect from NGC 4051 is an example of the “smooth” absorption morphology described in Kriss (2002). This morphology includes objects where the O VI absorption is so broad and blended that individual O VI components cannot be identified. Another NLS1 with a “smooth” O VI absorption morphology is Ark 564 (Romano et al. 2002). Other NLS1s have “single” morphology (like Ton S180 and IZw 1) or a “blend” morphology (like Mrk 478; see Kriss 2002 for details). Thus, NLS1s appear to be similar in their range of O VI absorption-trough morphologies to broad-line Seyfert 1s.

The deep absorption troughs imprinted on the O VI and C III broad emission lines indicate these absorbers reside at a distance from the AGN center larger than the corresponding broad line region (BLR) size. In NGC 4051 the BLR size has been measured, using optical Balmer lines, to be 3 ± 1.5 light days ($[7.8 \pm 3.9] \times 10^{15} \text{ cm}$; Shemmer et al 2003, see also Peterson et al. 2000). The BLR size for the UV lines (higher ionization lines) is known to be smaller than that of the optical lines (lower ionization lines) by a factor of $\sim 2-3$ (e.g.,

Peterson & Wandel 2000). This is attributed to the fact that the ionizing flux density is higher closer to the central source. Taking these considerations into account, we estimate a lower limit for the distance of the FUV absorber from the central continuum source to be $\sim 2 \times 10^{15}$ cm.

The amount of nuclear FUV/UV light scattered around the absorbing material and into our line of sight is practically zero since the absorption troughs of the low-ionization ions (H I, C III, C IV, and N V) reach saturation at zero flux. We find the higher ionization ion O VI to have a covering factor of ~ 0.9 – 0.95 . This might indicate that the higher ionization absorbers have a smaller covering factor than the low-ionization absorbers.

5.2. Ultraviolet — X-ray Connection

Several studies have suggested a link between the UV and X-ray absorbers in AGN (e.g., Mathur, Elvis, & Wilkes 1995; Crenshaw et al. 1999). The data presented in this paper enable us to examine this connection in NGC 4051.

In Figure 6 we compare the N V λ 1238 absorption from the STIS spectrum, the O VI λ 1038 absorption from the *FUSE* spectrum, and combined line profiles of He-like ions and H-like ions from the *Chandra* HETGS data (Figure 3 of Collinge et al. 2001). The resolution and S/N of the HETGS spectrum do not allow precise measurement of the X-ray absorption systems. The velocity shifts and FWHMs of the FUV and UV absorption systems are consistent with the low-velocity (~ 600 km s $^{-1}$) X-ray absorber which is seen in both the He-like and H-like lines.¹⁰ Both the He-like and the H-like profiles seem to extend to higher blueshift velocities than the FUV and UV absorbers; however, given the HETGS resolution and the poor S/N of the X-ray spectrum, it is not possible to determine the significance of this effect. We do not identify in the FUV and UV absorption lines the high-velocity absorption system (at -2340 km s $^{-1}$) observed in the X-ray spectrum by Collinge et al. (2001). In particular, we do not detect this system in O VI. The high-velocity absorption system in the X-ray spectrum was detected only in the H-like ions of Si, Mg, Ne and O; it is only marginally seen in the He-like ions of these elements (Figure 6c). Thus, it is not implausible that for the lower ionization ion O VI we do not detect this absorption system. Further observations, probably with *Chandra*, are required to investigate the putative -2340 km s $^{-1}$ absorption system further.

McHardy et al. (1995) and Nicastro et al. (1999) modeled *ROSAT* observations of NGC 4051 and claimed significant ionized X-ray absorption variability. Our observations, in contrast, fail to find any significant FUV absorption variability (though the limited temporal sampling might have caused a coincidence of observing on times when conditions were similar). This initially appears surprising if the UV and X-ray absorbers are connected. One possible explanation is that the low-resolution *ROSAT* data were confused by complex X-ray spectral variability; changes in the power-law continuum and/or soft excess could have created a false impression of ionized absorption variability. Alternatively, this could be attributed to FUV line saturation. Since most of the FUV absorption lines we detect appear saturated, changes in the ab-

¹⁰ We note that the profile of the low-velocity absorber has its main trough between ~ -500 and -900 km s $^{-1}$ in X-ray H-like lines, whereas in X-ray He-like lines it spans a wider range from ~ -100 to -900 km s $^{-1}$ (see Figures 6c and 6d). The more highly ionized absorber may be more concentrated at higher outflow velocities, or alternatively emission lines may be filling in the low-velocity part of the H-like absorption trough.

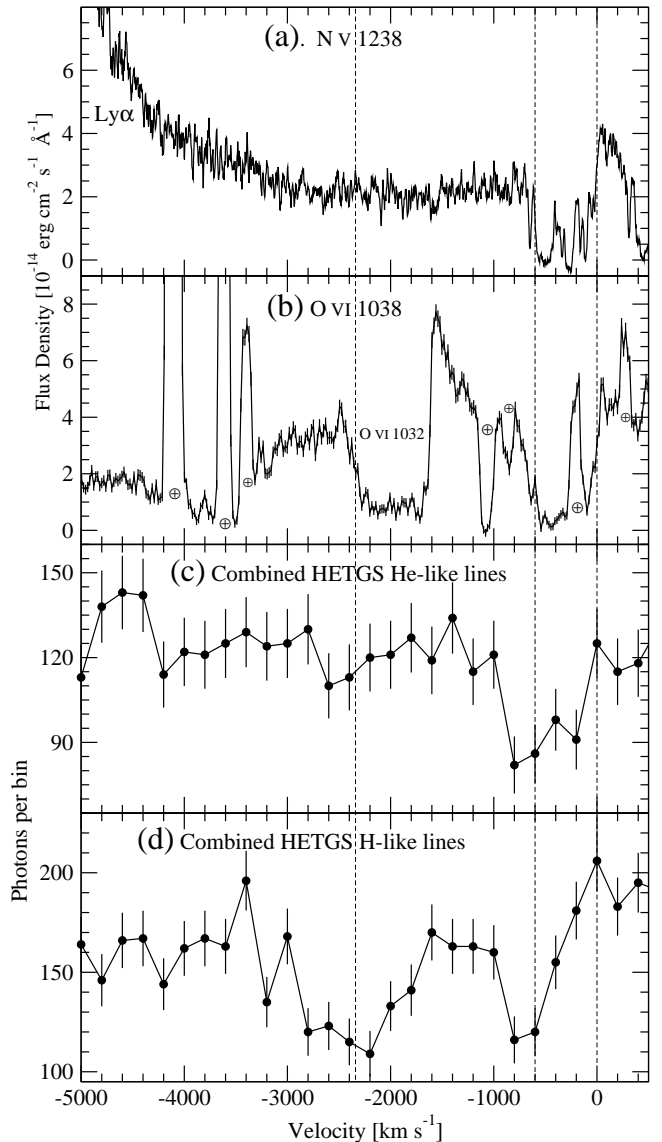


FIG. 6.— Line velocity profiles. (a) The N V λ 1238 absorption from the STIS spectrum. (b) The O VI λ 1038 absorption from the *FUSE* spectrum. (c) and (d) are the combined line profiles of He-like and H-like ions, respectively, from the *Chandra* HETGS data binned to 200 km s $^{-1}$ (Figure 3 of Collinge et al. 2001). The dashed vertical lines show 0 , -600 , and -2340 km s $^{-1}$ velocities. The wide absorption trough around -2000 km s $^{-1}$ in panel (b) is from O VI λ 1032. Airglow geocoronal emission lines and interstellar Galactic absorption lines are marked with \oplus .

sorber might lead to little change in the absorption lines. A possible exception is the C III absorption which does not seem to be heavily saturated; the lack of apparent C III absorption variability supports the idea that the absorber does not change substantially on time scales of months.

5.3. The Spectral Energy Distribution of NGC 4051

In Figure 7 we show a spectral energy distribution (SED) of NGC 4051 from the infrared to the X-ray. All data were corrected for the Galactic absorption (see caption for details), but no intrinsic reddening correction was applied. In the radio region (which is not shown in the figure) the object is radio quiet with $\nu F_\nu \approx 10^{-16}$ – 10^{-15} erg cm $^{-2}$ s $^{-1}$. The data we present are not contemporaneous, but overall most of the data represent an average over time of the object's flux (see the figure

TABLE 4
LUMINOSITY OF NGC 4051 IN SEVERAL BANDS

Wavelength [Å]	Data used	Luminosity [10^{40} erg s $^{-1}$]
4000–7500	Optical	61
1300–3300	<i>IUE</i>	37
1200–1700	STIS	11
950–1150	<i>FUSE</i>	3.8
6.2–24.8	HETGS	16
1.9–6.2	HETGS	13

NOTE. — Luminosity is computed using a cosmology of $H_0 = 70$ km s $^{-1}$ Mpc $^{-1}$, $\Omega_M = 0.3$, and $\Omega_\Lambda = 0.7$, which results in a luminosity distance of 9.8×10^6 pc to NGC 4051.

caption for details). The SED resembles the one presented in Komossa & Fink (1997), although here the SED is more detailed and has larger wavelength coverage.

The mean spectrum of NGC 4051 from the FUV to the optical is represented by data from four instruments and is averaged over timescales of years. The data from all four instruments are in good agreement (notable is the agreement of the STIS spectrum which is at a consistent flux level with the averaged *IUE* spectrum observed one-to-two decades before). The optical continuum of NGC 4051 varies little (e.g., Shemmer et al. 2003), the UV continuum is also consistent with little variation, and the current work shows that NGC 4051 did not vary significantly in the FUV. Nevertheless, there are notable variations in the optical line fluxes (e.g., Shemmer et al. 2003). Since the optical-to-FUV continuum does not vary much, a plausible conclusion is that the line variations are driven by the rapid and large soft X-ray and extreme UV variations and are not driven by the near or far UV as suggested before for this object.

The observed SED of NGC 4051 can be fitted with a power law ($f_\nu \propto \nu^\alpha$) in limited spectral ranges. We find α to be -1.46 ± 0.01 in the optical range (5500–7500 Å) and -2.03 ± 0.02 in the UV range (1160–3000 Å). The FUV cannot be fitted with a power law as it is contaminated by emission and absorption, though Figure 7 suggests the UV slope continues into the FUV. In the X-ray range we find from the HETGS spectrum in the range 2–6 keV that $\alpha = -0.84 \pm 0.04$. In Table 4 we give the luminosity of NGC 4051 in several bands assuming $H_0 = 70$ km s $^{-1}$ Mpc $^{-1}$, $\Omega_M = 0.3$, and $\Omega_\Lambda = 0.7$.

Overall the SED shows a gradual rise in the emitted energy from the hard X-rays to the far-IR. Most of the observed energy from NGC 4051 is seen in the far-IR, while the FUV emission is about an order of magnitude weaker. The UV and FUV spectra do not show indications for a big blue bump. Such an observed SED could be explained by dust along the line of sight which reddens the optical-to-FUV spectrum and re-emits energy in the far-IR. This would be similar to the observed SED of Ark 564 in which significant reddening was found (Crenshaw et al. 2002; Romano et al. 2003). However, data from *EUVE* and *ROSAT* strongly constrain the amount of cold gas along the line of sight that could be associated with the putative dust (e.g., McHardy et al. 1995; Uttley et al. 2000). One solution to this difficulty could be to invoke an ionized absorber with embedded dust (e.g., Brandt, Fabian, & Pounds 1996; Kraemer et al. 2000), although even in this case there is little evidence at present for X-ray absorption edges from the dust grains themselves (e.g., Komossa & Fink 1997). Also, the relatively high flux in the far-IR could have a significant contribution from the host galaxy (e.g., Ward et al. 1987; Elvis et al. 1994).

Further evidence against a dust-reddening interpretation comes from consideration of the He II $\lambda 1640/\lambda 4686$ ratio. We estimate the observed ratio to be a surprisingly high 19.2 ± 6.3 from a STIS measurement of the He II $\lambda 1640$ line [$(2.5 \pm 0.3) \times 10^{-13}$ erg cm $^{-2}$ s $^{-1}$; Collinge et al. 2001] and a ground-based measurement of the He II $\lambda 4686$ line [$(1.3 \pm 0.4) \times 10^{-14}$ erg cm $^{-2}$ s $^{-1}$; Peterson et al. 2000]. Such a value is not supportive of a reddening interpretation which predicts the ratio to be $\lesssim 9$ (compare with Crenshaw et al. 2002). If the continuum is reddened then the absorption at 1640 Å is ~ 10 times larger than at 4686 Å (by comparing the observed local-continuum flux ratio in Figure 7 to what is seen in a normal AGN). Such absorption would be expected to produce a He II $\lambda 1640/\lambda 4686$ ratio of ~ 1 . While our measured line ratio should be treated with caution since variability can add a factor of ~ 2 to the uncertainty, it still seems significantly higher than the expected ratio from reddening. More accurate and simultaneous measurements of this and other line ratios are needed to confirm this result.

An alternative to models with significant reddening is that, perhaps due to its low black hole mass (Shemmer et al. 2003), NGC 4051 may have a high-temperature big blue bump that is not apparent even in the FUV (compare our Figure 7 with Figure 3 of Puchnarewicz et al. 1995). Discrimination between significant reddening and a high-temperature big blue bump is challenging, and we leave this task to a future study. For example, it will be necessary to determine unambiguously if the observed excess soft X-ray emission is due to a continuum soft X-ray excess (e.g., Collinge et al. 2001) or a relativistically broadened O VIII recombination spectrum (Ogle et al. 2004).

6. SUMMARY

Using three *FUSE* observations, we have presented the first measurements of the FUV spectral and variability properties of the intensively studied NLS1 NGC 4051. Our main results are the following:

1. NGC 4051 shows no significant FUV variability in either its continuum or line properties during three epochs spanning about one year.
2. We detect FUV emission lines from O VI, N III, C III, and He II as well as blueshifted absorption lines from O VI, C III, and H I.
3. The FUV absorption is generally coincident in velocity with the UV absorption seen by STIS, although the lower FUV spectral resolution limits our ability to resolve all of the absorption complexity seen in the UV. There is no evidence for new velocity components seen only in higher ionization FUV lines.
4. The FUV absorption appears coincident in velocity with only the lowest velocity (-600 km s $^{-1}$) X-ray absorption system known. The several claimed X-ray absorption systems at higher velocities are not detected in the FUV, although this does not rule out the existence of these systems.
5. The H I Lyman series absorption lines are detected up to the Lyman edge, and two main velocity systems are seen in these lines. Column density estimates for these two systems indicate that the H I column density is lower for systems with larger outflow velocities. A possible third velocity system is also seen.

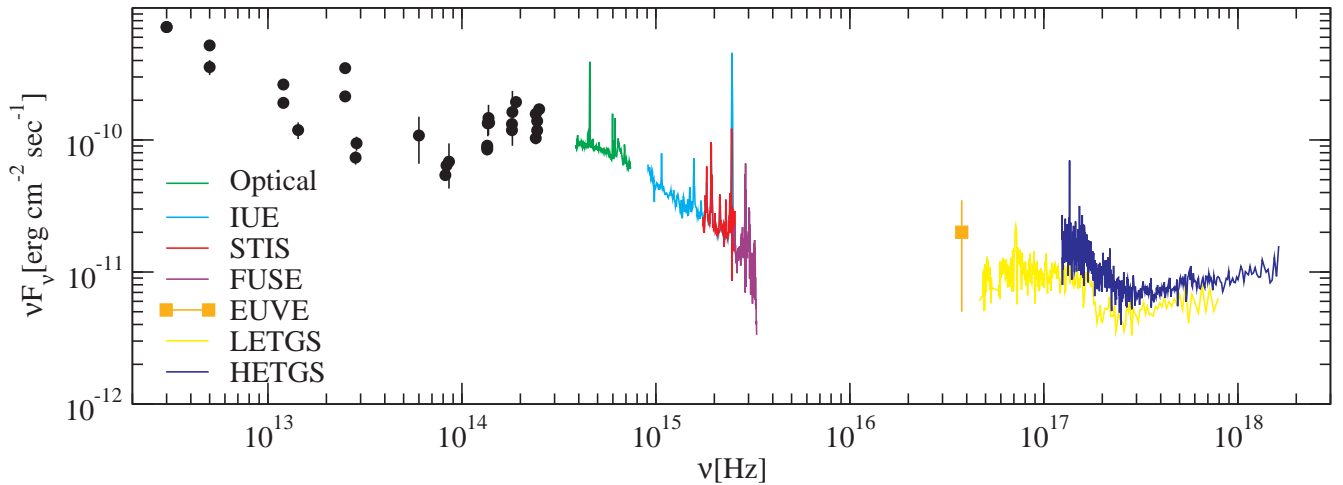


FIG. 7.— The SED of NGC 4051. Optical data are the average spectrum from Shemmer et al. (2003). *IUE* data are mean archive spectra taken over ~ 10 yr. The *FUSE* data are the average spectrum from this work. *EUVE* data are from Uttley et al. (2000), and the error bar represents the variability range. *STIS* and *HETGS* data are from Collinge et al. (2001); the *HETGS* data represent an average of the high and low states. The *LETGS* data are reported by van der Meer et al. (2003) and were taken while NGC 4051 was in a lower X-ray flux state. The spectra were heavily binned for clarity. The infrared data were taken from the NASA Extragalactic Database (NED) and were obtained by *IRAS* in the far-IR and ground-based observatories in the near-IR. The data were corrected for the Galactic absorption, even though it is low. We used $E(B - V) = 0.013$ mag and the extinction curve of Cardelli, Clayton, & Mathis (1989) for the UV to IR spectra, and $N_{\text{H}} = 1.3 \times 10^{20} \text{ cm}^{-2}$ (Elvis, Wilkes, & Lockman 1989) with the *WABS* model in *XSPEC* (Morrison & McCammon 1983) for the X-ray spectra. No intrinsic reddening correction was applied.

6. Any line-of-sight acceleration of the FUV absorption is constrained to be $\lesssim 1 \text{ mm s}^{-2}$.
7. The deep absorption troughs imprinted on the O VI and C III broad emission lines indicate that the FUV absorbing material resides at least $\sim 2 \times 10^{15} \text{ cm}$ from the central continuum source.
8. Several low-ionization ions have troughs that reach saturation at zero flux, significantly constraining the amount of nuclear FUV/UV light scattered around the absorbing material.

We thank D. Chelouche, A. Laor, H. Netzer, O. Shemmer, and P. Uttley for helpful discussions and sharing data. We are grateful for several valuable suggestions by I. M. McHardy. We gratefully acknowledge the financial support of NASA grant NAG5-13010, Israel Science Foundation grant 545/00 (S. K.), NASA LTSA grant NAG5-13035 (W. N. B.), an NDSEG Fellowship (M. J. C.), and the National Science Foundation under grant AST0205990 (C. S. R.). This research has made use of the NASA/IPAC Extragalactic Database (NED) which is operated by the Jet Propulsion Laboratory, California Institute of Technology, under contract with NASA.

REFERENCES

- Arav, N., Korista, K. T., & de Kool, M. 2002, *ApJ*, 566, 699
 Brandt, W. N., Fabian, A. C., & Pounds, K. A. 1996, *MNRAS*, 278, 326
 Cardelli, J. A., Clayton, G. C., & Mathis, J. S. 1989, *ApJ*, 345, 245
 Collinge, M. J. et al. 2001, *ApJ*, 557, 2
 Crenshaw, D. M., Kraemer, S. B., Boggess, A., Maran, S. P., Mushotzky, R. F., & Wu, C. 1999, *ApJ*, 516, 750
 Crenshaw, D. M. et al. 2002, *ApJ*, 566, 187
 de Vaucouleurs, G., de Vaucouleurs, A., Corwin, H. G., Buta, R. J., Paturel, G., & Fouque, P. 1991, Third Reference Catalogue of Bright Galaxies (New York: Springer)
 Elvis, M., Wilkes, B. J., & Lockman, F. J. 1989, *AJ*, 97, 777
 Elvis, M. et al. 1994, *ApJS*, 95, 1
 Feldman, P. D., Sahnou, D. J., Kruk, J. W., Murphy, E. M., & Moos, H. W. 2001, *J. Geophys. Res.*, 106, 8119
 Gabel, J. R. et al. 2003, *ApJ*, 595, 120
 Hubble, E. P. 1926, *ApJ*, 64, 321
 Komossa, S., & Fink H. 1997, *A&A*, 322, 719
 Kraemer, S. B., George, I. M., Turner, T. J., & Crenshaw, D. M. 2000, *ApJ*, 535, 53
 Kriss, G. 2002, in X-ray Spectroscopy of AGN with Chandra and XMM-Newton, eds. Boller, T., Komossa, S., Kahn, S., Kunieda, H., & Gallo, L. (Garching: MPE), p. 109
 Lamer, G., McHardy, I. M., Uttley, P., & Jahoda, K. 2003, *MNRAS*, 338, 323
 Mar, D. P. & Bailey, G. 1995, *Publications of the Astronomical Society of Australia*, 12, 239
 Marshall, F. E., Holt, S. S., Mushotzky, R. F., & Becker, R. H. 1983, *ApJ*, 269, L31
 Mathur, S., Elvis, M., & Wilkes, B. 1995, *ApJ*, 452, 230
 McHardy, I. M., Green, A. R., Done, C., Puchnarewicz, E. M., Mason, K. O., Branduardi-Raymont, G., & Jones, M. H. 1995, *MNRAS*, 273, 549
 McHardy I. M., Papadakis I. E., Uttley P., Page M. J., & Mason K. O., 2003, *MNRAS*, in press (astro-ph/0311220)
 Moos, H. W. et al. 2000, *ApJ*, 538, L1
 Morrison, R. & McCammon, D. 1983, *ApJ*, 270, 119
 Nicastro, F., Fiore, F., Perola, G. C., & Elvis, M. 1999, *ApJ*, 512, 184
 Ogle, P. M., Mason, K. O., Page, M. J., Salvi, N. J., Cordova, F. A., McHardy, I. M., & Priedhorsky, W. C. 2004, *ApJ*, in press (astro-ph/0401173)
 Peterson, B. M. & Wandel, A. 2000, *ApJ*, 540, L13
 Peterson, B. M. et al. 2000, *ApJ*, 542, 161
 Pounds, K. A., Reeves, J. N., King, A. R., & Page, K. L. 2003, *MNRAS*, in press (astro-ph/0310257)
 Puchnarewicz, E. M., Mason, K. O., Siemiginowska, A., & Pounds, K. A. 1995, *MNRAS*, 276, 20
 Pradhan, A. K. 2000, *ApJ*, 545, L165
 Richards, G. T., Vanden Berk, D. E., Reichard, T. A., Hall, P. B., Schneider, D. P., SubbaRao, M., Thakar, A. R., & York, D. G. 2002, *AJ*, 124, 1
 Rodriguez-Pascual, P. M., Mas-Hesse, J. M., & Santos-Lleo, M. 1997, *A&A*, 327, 72
 Romano, P., Mathur, S., Pogge, R. W., Peterson, B. M., & Kuraszkiewicz, J. 2002, *ApJ*, 578, 64
 Romano, P. et al. 2003, *ApJ*, in press (astro-ph/0311206)
 Sahnou, D. J. et al. 2000, *ApJ*, 538, L7
 Sembach, K. R. 1999, *ASP Conf. Ser.* 166: Stromlo Workshop on High-Velocity Clouds, eds. Gibson, B. K. & Putman, M. E., 243
 Seyfert, C. K. 1943, *ApJ*, 97, 28
 Shemmer, O., Uttley, P., Netzer, H., & McHardy, I. M. 2003, *MNRAS*, 343, 1341
 Uttley, P., McHardy, I. M., Papadakis, I. E., Cagnoni, I., & Fruscione, A. 2000, *MNRAS*, 312, 880
 van der Meer, R. L. J., Kaastra, J. S., Steenbrugge, K. C., & Komossa, S. 2003, *ASP Conf. Ser.* 290: Active Galactic Nuclei: From Central Engine to Host Galaxy, 133
 Ward, M., Elvis, M., Fabbiano, G., Carleton, N. P., Willner, S. P., & Lawrence, A. 1987, *ApJ*, 315, 74